Electromechanical Impedance Tomography for Soft Tactile Sensor

Shunsuke Yoshimoto [1]

[1] The University of Tokyo, Japan
Keywords: Tactile Imaging, Tomography, Pressure Distribution, Touch Sensing, Haptics.

ABSTRACT

This study introduces a tactile sensing technology based on a tomographic approach with conductors for imaging of pressure distribution. The sensor comprises electromechanically coupled driving and probing conductors. This system utilizes voltage sets from electrodes on the border of the probing conductor to solve an inverse problem for estimating electrical boundary conditions. The proposed technology enabled designing the soft tactile sensor, characterized by high positional accuracy, adjustable sensitivity and range, and a relatively simple fabrication process.

1 INTRODUCTION

Tactile sensing is an emerging technology for detecting mechanical interaction between a human, a robot, and the environment. The use of tactile imaging technology to visualize pressure or stress distribution on an object is valuable for indicating appropriate behavior in sports training, mobile biomonitoring in medical diagnostics and health care, and stably grasping an object using a robotic hand [1,2]. Several sensing methods have been proposed for detecting mechanical interaction with high accuracy, wide dynamic range, and quick responsiveness.

Tactile imaging involves two approaches: contact and non-contact. The contact sensing approach typically uses an array-type or matrix-type element of pressure sensitive structures [3,4]. The non-contact sensing approach rather employs a camera-based method, that is effective for detecting the deformation and strain image with high resolution [5]. A technical challenge currently facing tactile imaging technologies is establishment of a soft sensor that is easily customized for various surface. A simple tactile sensor with few wires is desired for the flexibility of implementation.

Electrical Impedance Tomography (EIT) is a technology for imaging the impedance distribution of an object. It involves scanning potentials at various excitation conditions using multiple electrodes located on the border of the object [6]. The use of a pressure sensitive conductor enables the application of EIT is for pressure imaging [7,8]. Since the EIT-based tactile sensor requires a smaller number of the electrodes compared to the array and matrix-type sensors, the method offers high sensor design flexibility. However, previous EIT-based tactile sensors exhibit low sensitivity and the fabrication process is complex.

To overcome these difficulties, the author proposes proposed a tomographic approach based on electromechanically coupled conductors for visualizing pressure distribution [9]. The method produces high positional accuracy, adjustable sensitivity and range, and an easy fabrication process. A summary of the proposed sensing method and implementation examples are provided.

2 SENSING METHOD

The electrical contact impedance, specifically resistance, between conductors changes according to the contact pressure. The application of voltage to a conductor also causes potential distribution relative to the electrical boundary condition. A tomographic approach is therefore employed for estimating pressure distribution using potential data sampled from multiple locations on a conductor. The detector structure, circuit design, reconstruction algorithm, and pressure estimation are explained in subsequent sections.

2.1 Detector structure

The detector structure resembles the resistive film system of a touch panel, comprising driving and probing layers. The driving layer is connected to a DC voltage source while the probing layer is connected to the multiple sensing electrodes surrounding the layer boundary. The two layers are isolated by a small insulator like a micro dot separator for the zero-contact state. Contact is established between the layers when pressure is applied to the detector. Although resistive coupling is employed to simplify circuit design, capacitive coupling is also effective.

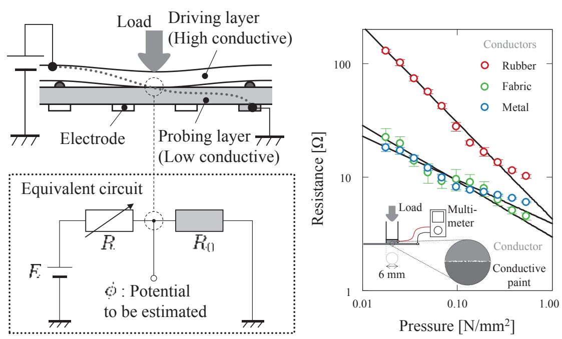

(a) (b)

Fig. 1 Structure of the detector and contact resistance (modified from [9]).

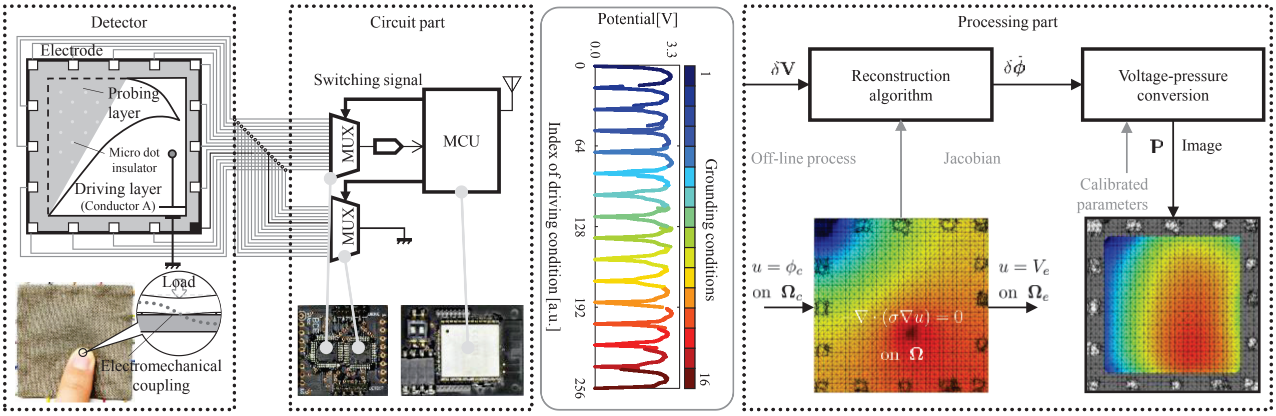

Fig. 2 Overview of the proposed tactile imaging system (modified from [9]).

Considering the circuit in Fig. 1(a), the potential ϕ at the contact region is represented by the following equation:

$$\phi = E\frac{R_0}{R_0 + R} \quad (1)$$

where E is the applied voltage, R_0 is the resistance of the conductor, and R is the contact resistance. The relationship between the contact pressure P and the electrical resistance R is expressed as follows:

$$R = \alpha P^{\gamma} \quad (2)$$

where α and γ are constants related to the shape and material of the conductor. Fig. 1(b) shows the measured data fits well into the model.

2.2 Sensing circuit

The sensing circuit differs from previous EIT-based tactile sensors regarding the connection of the voltage source. A DC voltage source is connected to the driving layer and reference electrodes are connected to the probing layer. The sensitivity of the detector is adjusted through the selection of the resistance for the probing and driving layers. Since the contact pressure induces a large change in contact impedance, the proposed system requires no amplifier. The sensing circuit comprises two multiplexers and a microcontroller. One multiplexer is for switching a grounding electrode while the other is for switching a sensing electrode.

2.3 Reconstruction algorithm

This system estimates the electrical boundary condition after acquiring voltages for all grounding conditions. To order to define the inverse problem, the forward problem calculating the potential at each electrode for an electrical boundary condition is introduced. The potential distribution u on a steady-state conductive body Ω follows the Laplacian elliptic partial differential equation given as:

$$-\nabla \cdot (\sigma \nabla u) = 0 \quad \text{on } \Omega \quad (3)$$

where σ is conductivity of the object. Then, electrical boundary condition is given as follows:

$$u = \phi_c \quad \text{on } \Omega_c, \quad u = 0 \quad \text{on } \Omega_g \quad (4)$$

where, Ω_c and Ω_g are the contact and grounded regions, respectively. The forward problem is to getting the potential u at each electrode region Ω_e with the boundary condition. In this study, the detector is represented by a thin shell mesh and FEM is used to solve the forward problem. Consequently, the electrode potential vector $\boldsymbol{V}$ is given as follows:

$$\boldsymbol{V} = \mathbf{J}\boldsymbol{\phi} \quad (5)$$

where $\boldsymbol{\phi}$ is a boundary potential vector and $\mathbf{J}$ is a Jacobian matrix.

The Jacobian matrix is expressed by the derivative of the input potential, i.e., the electrical boundary condition. Each component of the Jacobian matrix is obtained by computing the equation expressed as follows:

$$J_{i,k} \approx \frac{\partial V_i}{\partial \phi_k}; i = 1 \dots ML; k = 1 \dots K \quad (6)$$

where M is the number of electrodes, L is the number of grounding conditions, and K is the number of elements of the FEM mesh. To estimate potential distribution caused by the mechanical interaction, a solution to the inverse problem is required. A simple approach adopted to obtain an approximate solution of the inverse problem involved using the Tikhonov regularization deferential imaging technique [10]. Then, the inverse solution of the proposed system is expressed as follows:

$$\delta\tilde{\boldsymbol{\phi}} = (\mathbf{J}^{\mathrm{T}}\mathbf{J} + \lambda^2\mathbf{Q})^{-1}\mathbf{J}^{\mathrm{T}}\delta\boldsymbol{V} \quad (7)$$

where $\delta\boldsymbol{V}$ is the measured potential vector, $\delta\tilde{\boldsymbol{\phi}}$ is the estimated boundary condition vector, $\mathbf{Q} = \mathbf{I}$ is an identity matrix, andλ is a hyper parameter. Real time application requires calculation of the inverse matrix $(\mathbf{J}^{\mathrm{T}}\mathbf{J} + \lambda^2\mathbf{Q})^{-1}$ before the sensing.

2.4 Potential-pressure conversion

After determination of the electrical boundary condition is determined, calculation of the mechanical boundary condition is needed. Therefore, the pressure was estimated from the potential distribution. Since the electrical boundary condition involves a non-zero value outside the contact region, a thresholding process is required to extract the pressure on the contact region. Although the appropriate value is different between the sensor structure, 50 % of the maximum value is used for the threshold as a simple implementation. The pressure

P_k at the element k is expressed as follows:

$$P_k = \left(\frac{a_1}{\delta\tilde{\phi}_k^{\mathrm{th}}} + a_2\right)^{a_3} \tag{8}$$

where $\delta\tilde{\phi}_k^{\mathrm{th}}$ is the thresholded potential, a_1, a_2, a_3 are constants related to the structure and the electromechanical property of the detector.

3 RESULTS

This section provides an example of the sensor implementation, the fundamental performance of the sensing technique, and prospects of this study.

3.1 Implementation

Many possible factors for demonstrate the proposed sensing method exist. These include the shape of the detector, the materials used in the detector, and the number of electrodes. In this study, the simple implementation of a flexible sheet-type detector is introduced. The developed tactile sensor is shown in Fig. 3 (a) and (b). The sensor contains 16 copper electrodes, with conductive paint and fabric selected for the probing and driving layers, respectively. Also important is the use of a highly resistant material for the probing layer, whereas a low resistance material is suitable for the driving layer.

The sensing circuit comprises a microcontroller (ESP-WROOM-32, Espressif Systems), two analog multiplexers (ADG726, Analog Devices), and a 3.3 V lithium battery. The multiplexers were controlled using the digital outputs from the microcontroller. Because 16 electrodes were used, 256 voltage data points (16 electrodes × 16 conditions) were captured for estimating pressure distribution in a single frame.

Regarding the simulation of the potential distribution, a homogeneous triangular mesh of the detector was prepared. A typical example of the mesh contains about 6000 triangular elements and about 3000 nodes. Concerning the hyperparameter of the solver in Eq. (7), the L-curve and positional error were confirmed, with the optimized parameter λ^2 of 1000. To reduce the calculation cost in the online processing, a pseudo-inverse matrix was calculated during offline processing with the results of visualized pressure distribution (Fig.3 (c)).

3.2 Sensing Performance

The contact position and pressure were evaluated through a calibrated force sensor for assessment of the proposed method. The results show that the developed tactile sensor (60 mm × 60 mm) had a positional error of 3.49 ±1.56 mm had for the sheet length of 60 mm and pressure error of 0.0457 N/mm^2, with maximum pressure of 0.5 N/mm^2. Moreover, the results indicate that the positional accuracy depends on the sheet length and number of the electrodes.

The proposed tactile imaging method furnishes prominent pressure sensitivity and range, high positional accuracy, and ease of fabrication. A comparison of studies involving tomography or piezoelectrical transduction for tactile imaging is presented in Table 1. The proposed sensing method demonstrates a high localization accuracy compared to those in previous studies.

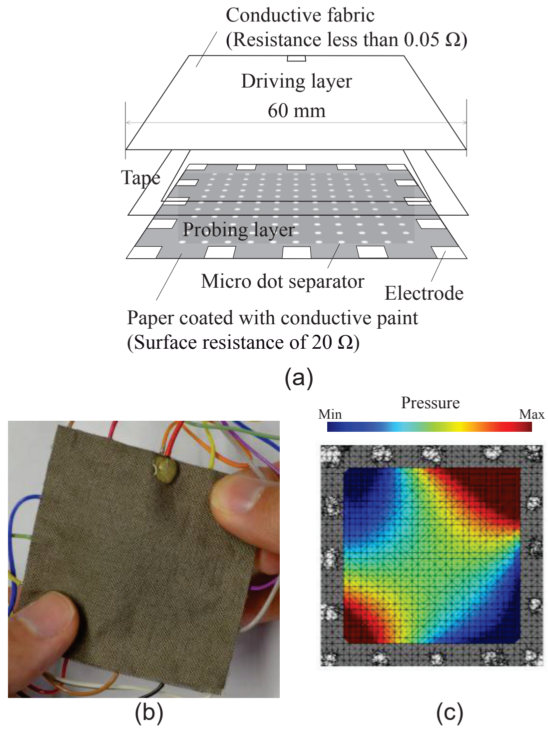

Fig. 3 Implementation of the sheet-type sensor.

The proposed method also does not require a pressure sensitive material. Therefore, the method is characterized by high shape design flexibility. Since the detector is scalable, the sensing circuit is applicable for micro to macro scale sensor sizes. Moreover, the proposed device consumes low power because current only flows during contact.

3.3 Prospects

The fundamentals of electromechanical impedance tomography using universal conductors are presented in this study. This technology is intended for industrial, medical, sports, and entertainment applications and ongoing developments include:

(1) Optimization of the transduction mechanism by investigating electrical contact mechanics of the conductive material.

(2) Extension of the sensing DoF, i.e., the sensing of shear stress distribution, by designing a functional surface structure between the conductors.

(3) Improvement in estimating the accuracy and resolution of pressure distribution by introducing state-of-the-art algorithm.

(4) Establishment of a fabrication process using novel technologies like flexible electronics.

Table 1 Comparison table for works using tomography or electromechanical coupling for tactile sensing

Transduction method	Material	Fabrication	Pressure (force) metrics	Spatial metrics
Electromechanical impedance tomography [9] (This study)	**Two conductors (universal)**	**Molding/ cutting/ printing/ painting (versatile)**	**Maximum 0.50 N/mm^2, 5.38–10.2% error rate, 147–163 dB SN**	**1.74 mm positional error in 30 mm × 30 mm area, 5.68 % positional error rate**
Piezoresistive [8] (neural network)	Nylon fabric, perforated cloth, and CNT-PDMS	Coating/ cutting	0.5–10 N range, Estimation R^2=0.875	7.02 mm positional error in 100 mm × 100 mm area (localization only)
Piezoresistive [11] (EIT)	Piezoresistive fabric	Cutting	NA	1.4–6.7 % positional error for single contact region
Capacitive array [3]	Synthetic polymer and metal alloy	Molding	42 dB dynamic range, 60 dB S/N	9 × 9 sensor array, 2 mm pitch
Piezoresistive array [4]	Piezoresistive fabric	Sewing	0.001–0.5 N/mm^2 range, 20–28% error rate	54 sensor array

4 CONCLUSIONS

A soft tactile imaging technique for measuring contact pressure distribution using the electrical contact resistance and a tomographic approach is proposed in this study. The proposed technology enables the design of the soft tactile sensor, characterized by high positional accuracy, adjustable sensitivity and range, and a relatively simple fabrication process. Therefore, the tactile imaging technology shows potential for the development of robotic intelligence, biomedical analysis, and human interfaces.

ACKNOWLEDGMENTS

This study was partially supported by the Japan Society for the Promotion of Science KAKENHI Grant Numbers JP16H05875 and JP19H04189.

REFERENCES

[1] M. Tiwana, S. Redmond, and N. Lovell, “A review of tactile sensing technologies with applications in biomedical engineering,” Sens. Actuators A Phys., vol. 179, pp. 17–31 (2012).

[2] R. Dahiya, G. Metta, M. Valle, and G. Sandini, “Tactile sensing-from humans to humanoids,” IEEE Trans. Robot., vol. 26, no. 1, pp. 1–20 (2010).

[3] B. Li, Y. Shi, A. Fontecchio, and Y. Visell, “Mechanical imaging of soft tissues with a highly compliant tactile sensing array,” IEEE Trans. Biomed. Eng., vol. 65, no. 3, pp. 687–697 (2018).

[4] G. H. Büscher, R. Kõiva, C. Schürmann, R. Haschke, and H. J. Ritter,“Flexible and stretchable fabric-based tactile sensor,” Rob. Auton. Syst., vol. 63, pp. 244–252 (2015).

[5] W. Yuan, R. Li, M. A. Srinivasan, and E. H. Adelson, “Measurement of shear and slip with a gelsight tactile sensor,” Proc. IEEE Int. Conf. Robot. Autom., pp. 304–311 (2015).

[6] M. Cheney, D. Isaacson, and J. C. Newell, “Electrical impedance tomography,” SIAM Rev., vol. 41, no. 1, pp. 85–101 (1999).

[7] D. Silvera-Tawil, D. Rye, M. Soleimani, and M. Velonaki, “Electrical impedance tomography for artificial sensitive robotic skin: A review,” IEEE Sens. J., vol. 15, no. 4, pp. 2001–2016 (2015).

[8] J. O’Neill, J. Lu, R. Dockter, and T. Kowalewski, “Stretchable, flexible, scalable smart skin sensors for robotic position and force estimation,” Sensors, vol. 18, no. 4, Art. no. E953 (2018).

[9] S. Yoshimoto, Y. Kuroda, and O. Oshiro, Tomographic Approach for Universal Tactile Imaging with Electromechanically Coupled Conductors. IEEE Trans. Ind. Elect., vol. 67, no. 1, pp. 627-636, 2020.

[10] A. Adler and R. Guardo, “Electrical impedance tomography: Regularized imaging and contrast detection,” IEEE Trans. Med. Imag., vol. 15, no. 2, pp. 170–179 (1996).

[11] S. Russo, S. Nefti-Meziani, N. Carbonaro, and A. Tognetti, “A quantitative evaluation of drive pattern selection for optimizing EIT-based stretchable sensors,” Sensors, vol. 17, no. 9, pp. 1999:1–16 (2017).